Lab on a Chip

PAPER

Microcapillary-assisted dielectrophoresis for single-particle positioning†

Yuan Luo,[a] Xu Cao,[b] Pingbo Huang[bcd] and Levent Yobas*[ac]

Here, we demonstrate microcapillary-assisted dielectrophoresis (µC-DEP), a new capability for precise positioning of particles or biological cells in applications such as dynamic assays. The method largely derives from a need to evade the challenges faced with hydrodynamic trapping of particles or cells at microcapillaries typically realized through brief application of suction. Microcapillaries here serve a dual purpose by firstly squeezing field lines to define localized positive DEP traps and then establishing an exclusive access to the trapped cell for probing. Strength of the traps is presented through numerical results at various excitation frequencies. Their effectiveness is shown experimentally against relevant solution conductivities using 10 µm polystyrene microspheres. Usefulness of the method for positioning individual cells is demonstrated *via* experimental results on cell viability and single-cell impedance spectroscopy.

Introduction

Microcapillary-based single-particle positioning has attracted a great deal of attention in the last decade from numerous biological applications including patch-clamp electrophysiology,[1–5] single-cell impedance spectroscopy,[6–9] and single-cell electroporation.[10] Such integrated microcapillaries offer sufficiently small openings (1–5 µm) that can immobilize individual cells for optical and/or electrical analyses and/or for intracellular delivery of materials (*e.g.*, drug compounds, nucleic acids). Docking cells to those openings is typically accomplished by suction pressure applied through the microcapillaries. This hydrodynamic trapping method, although it retains a simple platform, could lead to undesired consequences; possible trapping of nearby particulates along with cells or diluting the content of microcapillaries with cell buffer.[5] The latter may hamper the subsequent task to be performed on the trapped cell.[5]

Methods alternative to the hydrodynamic trapping involve field gradients that can induce external forces on cells including electric, electromagnetic, magnetic, and acoustic fields.[11] Acoustic fields lack the fine spatial resolution needed to position a single cell at a precise location while magnetic fields demand labeling cells with particles of magnetic susceptibility.

Electromagnetic fields, *i.e.*, optical tweezers, are capable of extremely high spatial resolution and yet require prior knowledge of cell position for tight focusing of a laser beam. Electric fields do not express these drawbacks and moreover scale favorably with microfluidics.[12] Cells can be mobilized through the interaction of their native or induced surface charge, respectively, with the field intensity (electrophoresis) or non-zero field gradient (dielectrophoresis). The former can be harmful to cells, as it maintains a constant voltage across them.

Dielectrophoresis (DEP), discussed more broadly in recent reviews,[12–14] traditionally uses spatially designed thin-film surface microelectrodes to induce the required non-uniform field. The technique has been extensively studied for the selective isolation and enrichment of target cell population from a mixture.[15] With the recent surge of interest in single-cell analyses, DEP has also been adopted for creating highly effective single-cell traps in various novel electrode designs including interdigitated,[16] ring,[17] and point-and-lid[18] configurations in addition to those more common quadrupole[19] and octopole[20] configurations.

DEP using surface microelectrodes suffer from electrode fouling, contamination, and bubble formation and the insulator-based DEP (iDEP) is a method proposed to bypass these issues.[21] Instead of integrating the electrodes, iDEP keeps them off the chip (external electrodes) and relies on the insulating boundaries of the flow chamber to confine the field into a non-uniform distribution. Thus, the method simplifies the fabrication process as well. Moreover, the influence of DEP can be felt across the entire chamber volume unlike the case with surface microelectrodes where the effect quickly dies off away from the surface. In return, the magnitude of the applied voltage has to be greatly increased to compensate the large separation between the external electrodes and to obtain field intensities and forces comparable to those with the surface microelectrodes. This high voltage may cause an excessive current flow through the sample

[a] Department of Electronic and Computer Engineering, Hong Kong University of Science and Technology, Clear Water Bay, Hong Kong SAR, China
[b] Division of Life Science, Hong Kong University of Science and Technology, Clear Water Bay, Hong Kong SAR, China
[c] Division of Biomedical Engineering, Hong Kong University of Science and Technology, Clear Water Bay, Hong Kong SAR, China.
E-mail: eelyobas@ust.hk
[d] State Key Laboratory of Molecular Neuroscience, Hong Kong University of Science and Technology, Clear Water Bay, Hong Kong SAR, China

and the subsequent joule heating, thereby limiting the choice of sample conductivity.

Contactless DEP (cDEP) avoids the complications arising from the sample-electrode interface (*e.g.*, bubble formation, fouling) by introducing a thin partition of insulating dielectric therein.[22,23] The field is coupled through the dielectric partition into the sample with a high-frequency voltage waveform applied across the electrodes. Also, the electrodes can be made of a highly conductive liquid (electrolyte) confined within isolated microchannels. Like iDEP, this allows cDEP to retain a simple fabrication process whereby a microfluidic layout for the electrodes and the sample chamber can be formed within a single process step. Unlike iDEP, though, the electrodes can be made lithographically close and in a desired layout to impose a non-uniform field distribution. Although both iDEP and recently cDEP have been demonstrated for selective separation of cells, neither has been implemented for a single-particle trap apart from a few recent studies.[24,25]

In this study, we investigate a single-particle dielectrophoretic trap defined by a microcapillary, presence of which greatly enhances localized field coupling through the dielectric partition. Such microcapillaries have already been in use for single-cell immobilization and analyses as articulated, albeit without eliciting DEP forces, whereas these forces could be favorable over hydrodynamic trapping of cells for two main reasons. First, DEP being selective to the size and dielectric properties of particles is likely to trap cells while excluding those interfering particulates (*e.g.*, cell debris). Second, DEP, operating through a field gradient instead of flow streams, may preserve the composition of the microcapillary filling. Thus, microcapillaries could serve a dual purpose; intensifying the field coupled to the sample while establishing an exclusive access to the trapped cell for electrical and/or fluidic probing.

Here, the capability of microcapillaries to induce pDEP forces for positioning single particles is studied mainly through beads as they exhibit more uniform electrical and physical characteristics. Non-uniform field distribution around the microcapillaries along with its gradient is analyzed using finite-element simulations for the assumed electrical boundary conditions. Statistics of a single-particle positioning are experimentally derived for various conductivity values of the solutions involved. Minimum trapping voltage is empirically determined for different flow speeds and excitation frequencies. Finally, the practicality of the method in positioning live cells is demonstrated for the single-cell impedance spectroscopy.

Theory

A spherical particle with radius (r) suspended in a medium exposed to a non-uniform electric field (E) feels a time-averaged DEP force:[26]

$$<F_{DEP}> = 2\pi\varepsilon_m r^3 \text{Re}[f_{CM}](\nabla E^2) \quad (1)$$

where ε_m is the absolute permittivity of the medium, and f_{CM} is Clausius-Mossotti (CM) factor. The CM polarization factor varies with the frequency of the field applied and depends on the complex permittivity of both the particle, ε_p^*, as well as the medium, ε_m^*, according to:

$$f_{CM} = \frac{\varepsilon_p^* - \varepsilon_m^*}{\varepsilon_p^* + 2\varepsilon_m^*} \quad (2)$$

A complex permittivity ε^* is related to the absolute permittivity ε, and the conductivity σ through:

$$\varepsilon^* = \varepsilon - j\sigma/\omega \quad (3)$$

where ω is the angular frequency of the field applied and j is $\sqrt{-1}$.

Real part of the CM factor, Re[f_{CM}], varies between -0.5 to $+1.0$ depending on the relative polarizability of the particle with respect to that of the surrounding medium. For Re[f_{CM}] > 0, the particle moves up the field gradient experiencing pDEP. For Re[f_{CM}] < 0, nDEP is observed as the particle moves down the field gradient.

Methods and materials

Reagents and buffers

For the electrodes in the bead experiments, a high conductivity solution was prepared by raising the level of NaCl in a concentrated 10 × PBS solution to bring the conductivity up to 150 mS cm^{-1}. All the remaining solutions had the following composition in deionized (DI) water in mM: 140 KCl, 2 CaCl$_2$, 2 MgCl$_2$, 20 HEPES, and 10 glucose. The solutions as prepared had a conductivity of 15 mS cm^{-1} and pH 5.25 and were further diluted with 300 mM mannitol solution to reduce the conductivity to the stated values (final pH 5.55). The conductivity and pH readings were taken *via* Mettler Toledo SevenGo Pro (Mettler-Toledo, Inc., OH). For staining cells, fluorescent dye Calcein-AM (Life Technologies, Inc., NY) was used.

Beads and cells

Carboxyl-modified fluorescence-stained polystyrene microspheres (Ø10 μm, FC07F, Bangs Laboratories, IN) were suspended in DEP medium according to the stated conductivities. Chinese hamster ovary K1 (CHO-K1) cells were cultured in F-12 K medium supplemented with 10% fetal bovine serum (FBS) in an atmosphere of 95% air-5% CO$_2$ at 37 °C. Cells were detached from the culture dishes by trypsin-EDTA treatment at 37 °C for 4 min. For staining, cells were incubated with a fluorescent dye of 4 μg mL^{-1} Calcein-AM (Life Technologies, Inc., NY) at 37 °C for 1 h. They were then washed twice and resuspended in DEP buffer solution (100 μS cm^{-1}) at a concentration of ∼1 × 10^6 cells mL^{-1}.

Instruments

The device under test was placed on the stage of an *epi*-fluorescence microscope (FN1; Nikon, Japan) equipped with a halogen lamp and a mercury lamp (100 W). Images were captured and stored in a computer through a CCD camera (R3 Mono; SPOT, MI) mounted on the microscope. A voltage signal of sine wave was applied to the device using copper wires from a high-voltage transformer (Amp-Line Corp., NY) driven by a function generator (CFG250, Tektronix, Inc., OR) through a

wideband power amplifier (AL-50HFA, Amp-Line Corp., NY). The waveform was monitored on an oscilloscope (2205GN, Tektronics Inc., OR). Impedance measurements were performed *via* an impedance analyzer (4294A, Agilent, CA).

Device fabrication

Microcapillaries were fabricated in polydimethylsiloxane (PDMS) through soft-lithography process (Fig. 1a). To form the template for microcapillaries, silicon ridge structures with nominal cross-section 2 μm by 2 μm were raised from the substrate surface through a deep reactive ion etching (DRIE).
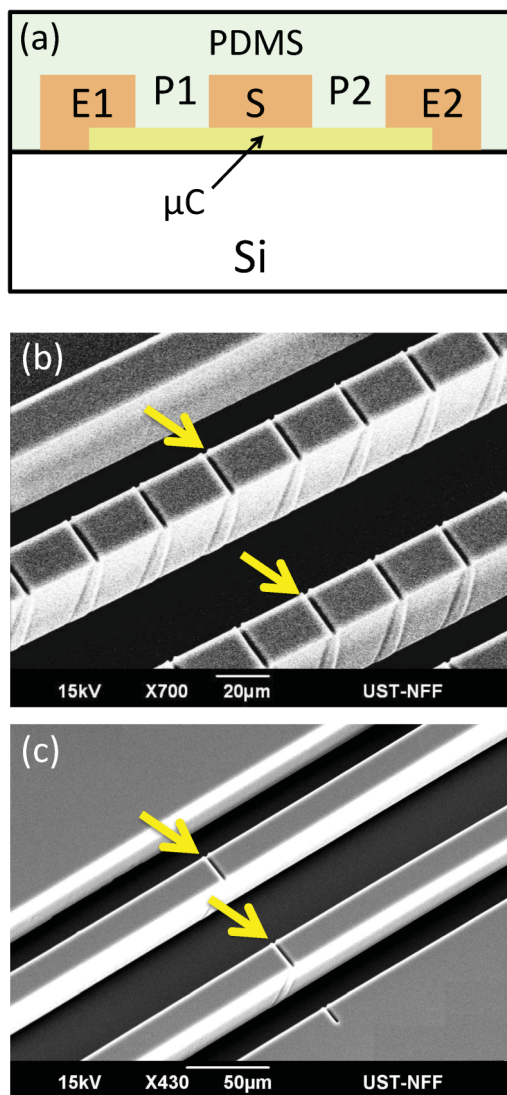

Fig. 1 (a) Cross-sectional schematic of a silicon template with a ridge microstructure μC for moulding microcapillaries in PDMS, SU-8 blocks E1, E2 and S for electrode reservoirs and a sample flow chamber, respectively. The gaps between them, P1 and P2, form PDMS partitions. SEM images of the designs characterized here with the microcapillaries shown facing up and un-bonded: (b) an array of microcapillaries (total 13) evenly spaced (30 μm apart) and (c) a single microcapillary on either partition. Arrows point at the representative microcapillaries. All the microcapillaries are identical with nominal dimensions 2 μm by 2 μm by 20 μm.

On the etched substrate, a layer of 45 μm-thick photoresist (SU-8, Microchem, MA) was subsequently patterned to form the template for deeper microchannel structures. Over the prepared template, PDMS elastomer (Sylgard 184, Dow corning, MI) was cured for half an hour at 120 °C after mixing and degassing the base material and the curing agent (10 : 1 w/w). The cured PDMS was peeled off, punched with inlet/outlet holes, and then permanently bonded over a glass slide upon activating their surfaces *via* oxygen plasma (40 W, 40 s).

Device designs

Each device accommodated a straight microchannel 50 μm wide for sample flow and separated from two outer microchannels, 30 μm wide, *via* PDMS dielectric partitions, 20 μm wide. The outer microchannels were loaded with conductive solutions for the electrodes and extended along the center microchannel such that the field induced by cDEP was uniform exerting a limited force only. To exert DEP forces on particles (beads or cells), a non-uniform field distribution was introduced locally by in-plane microcapillaries built into the partitions. On either partition, an array of microcapillaries, in total 13 evenly spaced apart by 30 μm, was situated in one particular design (Fig. 1b) and a single microcapillary in another design (Fig. 1c). The microcapillaries were all identical with their nominal dimensions 2 μm by 2 μm by 20 μm.

Device characterization

For experiments, the two outer microchannels and the microcapillaries were filled with the electrode solution at the indicated conductivities. Subsequently, bead or cell suspension was introduced into the center microchannel through plastic tubings inserted into the inlet/outlet holes. A syringe pump (Harvard Apparatus, MA) was used to control the flow rate. A pair of metal electrodes (copper wires for DEP activation and Ag/AgCl wires for impedance measurements) were placed into the reservoirs of the outer microchannels and then connected to the power supply or impedance analyzer.

Simulation

Using the AC/DC Module of COMSOL Multiphysics Software 3.4 (Comsol Inc., MA), the potential distribution ϕ across the device geometry was simulated by solving Laplace equation:

$$\nabla \cdot (\sigma^* \nabla \phi) = 0 \tag{4}$$

where σ^* is the complex conductivity given by $\sigma^* = \sigma + j\omega\varepsilon$ at the specified coordinates. Conductivity values were set as 15 mS cm^{-1} for the electrolyte, 100 μS cm^{-1} for the sample medium, and 0.8×10^{-8} μS cm^{-1} for the PDMS dielectric. Relative electrical permittivity was assigned as 80 for all the aqueous solutions and 2.65 for the PDMS dielectric. For the electrical boundary conditions, the potential at an inlet of an outer microchannel (supplying the microcapillaries) was set either at zero (ground) or at the prescribed voltage magnitude and frequency. Based on the simulated potential distribution, ϕ, the electric field $E = -\nabla\phi$ and its gradient $\nabla E = \nabla(-\nabla\phi)$ were calculated.

Results and discussion

Simulations

Fig. 2a shows a contour plot of the electric field intensity simulated across the design with an array of microcapillaries (shown only for one of the two partitions having four microcapillaries). Boundary conditions for the respective electrodes were assigned to be 0 and 35 V-rms (root mean squared) at 500 kHz. As can be noticed, the field gradient is highly intensified around the trap locations where the microcapillaries join the microchannel. This is also evident from the line plots where the gradient of the square of the field tends to peak near

Fig. 2 (a) A contour plot of the electric field simulated across the microcapillary array shown for the four adjacent microcapillaries. The dashed line delineates the coordinates along which the gradient of the square of the simulated field is presented in the subsequent line plot, (b) for three distinct excitation frequencies (legend) at 35 V-rms. (c) The line plot simulated after replacing the array of microcapillaries with a single microcapillary in various dimensions of width and length (legend) for an excitation frequency 150 kHz at 35 V-rms.

the traps (Fig. 2b). The magnitudes are in the order of 10^{14} (V^2 m^{-3}) being one or two orders larger than those of cDEP induced through PDMS partitions of a similar thickness. Yet, they can be achieved here through a fraction of the excitation voltage applied in comparison. This enhancement can be attributed to the presence of the microcapillaries and their, despite fairly small cross-sectional profiles, effective *conductive* coupling to the sample microchannel. Each microcapillary imposes an electrical resistance of ∼3.3 MΩ.

The microcapillaries play a crucial role in forming highly localized traps because not only do they effectively couple the field through the dielectric partitions but also considerably distort its distribution into a non-uniform profile (Fig. 2a). Without the presence of the microcapillaries, the dielectric partitions, as they stand, cannot have a notable impact on the field gradient solely based on their *capacitive* coupling (cDEP) since they project a uniform field of a parallel-plate capacitor. This can be seen through the line plot of Fig. 2b where the field gradient varies inversely with the excitation frequency at 35 V-rms. As the excitation frequency is increased from 150 kHz to 500 kHz, the *capacitive* coupling through the dielectric partitions begins to take over the *conductive* coupling through the microcapillaries. As a consequence, more and more field lines get penetrated through the dielectric partitions than those being squeezed through the microcapillaries. At 500 kHz, this results in a relatively uniform field and thus a reduced field gradient around the microcapillaries in the sample microchannel. Increasing the magnitude of the excitation voltage restores the strength of the traps (not shown).

Physical dimensions of the microcapillaries determine the force and effective area of a particle trap projected to the sample microchannel. Fig. 2c shows the simulated line plot after replacing the array of microcapillaries with an isolated microcapillary on each PDMS partition. The curves correspond to a particular combination of width and length values assigned to the microcapillary. A relatively low excitation frequency (150 kHz) is chosen to reduce the capacitive effects that might overshadow the influence of the microcapillary. A cursory comparison between Fig. 2b and 2c reveals that the force, proportional to the field gradient, induced by an isolated microcapillary is at least an order of magnitude larger than that by an array despite the same excitation frequency and magnitude (35 V-rms) applied. This is because the microcapillaries positioned closely, superpose their individual fields and reduce the local variations within the overall field distribution. Accordingly, the field gradient as well as the force is considerably reduced. In contrast, a drastic increase in the field gradient is observed in the vicinity of an isolated microcapillary opening which influences an area of 20–40 μm in radius.

Fig. 2c suggests that the field gradient or trapping force is correlated with the width or cross-sectional area of a microcapillary more strongly than its length. For instance, the field gradient is only slightly increased near a 2 μm-wide microcapillary upon a major reduction in its length from 40 μm to 10 μm whereas a more dramatic increase can be noticed for a 20 μm-long microcapillary with an increase in its width from 1 μm to 4 μm. This can be explained by the fact that the width or cross-sectional area of a microcapillary determines not only the field magnitude within a trap by limiting the voltage, but also the
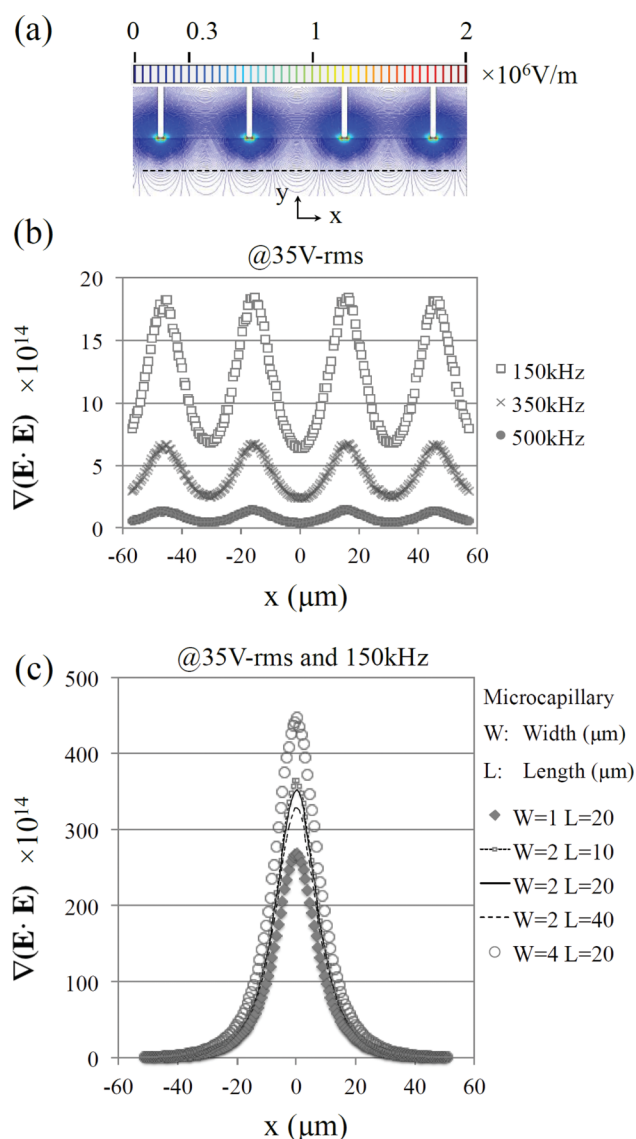
field gradient by confining the field lines. In contrast, the length of a microcapillary, once it exceeds its width, cannot effectively distort the field lines although it continues to limit the voltage and hence the field magnitude. Based on the same argument, the field gradient or the force cannot constantly increase with the width or cross-sectional area of a microcapillary as the width exceeding a certain size limit would distort the field lines less and less. Our simulations suggest an upper limit of $\sim 10~\mu m$ for the width of a 20 μm-long microcapillary beyond which the force begins to decline. This value is relatively large for the applications involving typical cells or particles.

Bead experiments

Microcapillary array. On the simulated geometry, we investigated trapping efficiency of 10 μm polystyrene beads as a function of the conductivity of the solutions loaded on the either side of the microcapillaries. Knowing that the magnitude of pDEP force quickly diminishes with the increased conductivity of the medium, we initially performed the experiments under the conditions that favor DEP: an extremely low conductivity for the bead suspension (1 $\mu S~cm^{-1}$) and a fairly high conductivity for the electrodes (150 $mS~cm^{-1}$). When we applied a voltage waveform of 71 V-rms at 500 kHz for a brief period (<1 min), we observed a strong pDEP force acting on the beads, trapping them as they moved along the microchannel. A representative image is shown in Fig. 3a and the beads can be seen trapped along the sidewalls either at the microcapillaries or the spaces between them.

To bring the conductivity values relevant to the target biological applications, we repeated the experiments with various bead suspensions prepared over a large conductivity range (extending three orders of magnitude) and with an electrolyte solution of reduced conductivity ($\sim 15~mS~cm^{-1}$). To compare the trapping performance among the experiments, we determined the average number of beads captured per microcapillary inclusive of those trapped between the microcapillaries. On average, around two beads per microcapillary could be captured with no significant degradation in the performance over the conductivity range of the bead medium tested up to 1 $mS~cm^{-1}$ (Supplementary, Fig. S1†). In a medium of 1 $mS~cm^{-1}$, the beads, however, could not be captured with the reduced electrode conductivity of 15 $mS~cm^{-1}$.

Single microcapillary. Noticing that the beads could also be trapped at the sites without any microcapillary, we then characterized a design with either partition presented with only a single microcapillary. Applying the same excitation voltage (71 V-rms 500 kHz), we monitored the patterns of bead trapping under pDEP. We witnessed a random trapping of a single bead, a pair of beads, or a few beads (mostly <4) in a group occurring all at the microcapillaries, as shown in Fig. 3b. Unlike the array design, we encountered under no circumstances trapping of beads off the microcapillaries. This suggests that the beads trapped at the adjacent microcapillaries may perturb the local field and create new trapping sites between the microcapillaries, the so-called "pearl-chain" formation.[26,27]

With a single microcapillary on each partition, we investigated trapping statistics of beads as a function of the conductivity
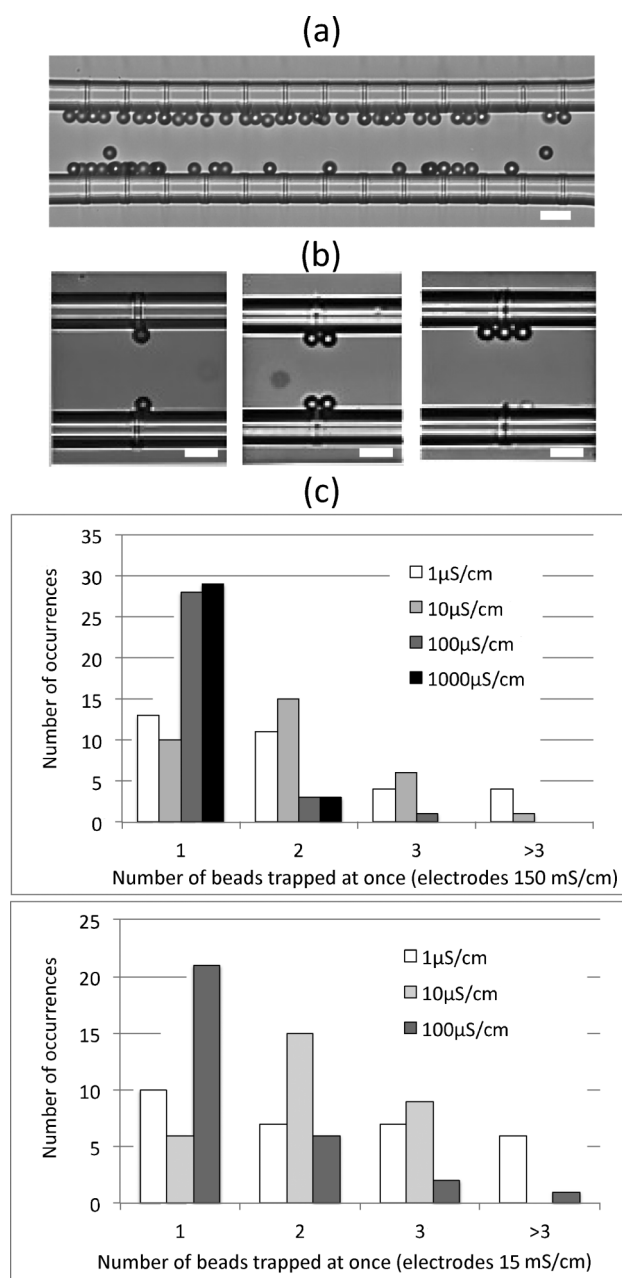

Fig. 3 Photomicrographs of 10 μm beads trapped by (a) a microcapillary array and (b) a single microcapillary (successive images showing increased number of beads randomly trapped at once). Scale bar: 20 μm in all. (c) Plots showing trapping statistics of beads at a single microcapillary for the selected conductivity values of the bead medium (the figure legends) and of the electrodes. In all, an excitation voltage of 71 V-rms at 500 kHz was applied to induce pDEP.

values of the solutions. Results are presented through plots showing number of occurrences in Fig. 3c. With the electrodes defined by a high conductivity electrolyte (150 $mS~cm^{-1}$) and the suspension medium ranging from 100 $\mu S~cm^{-1}$ to 1000 $\mu S~cm^{-1}$, beads are more likely to get trapped individually as opposed to in groups (pairs or more). In these conductivities, a group of beads ($\geqslant 3$) was encountered in a trap only on rare cases whereas they were not uncommon with a lower conductivity medium (1 $\mu S~cm^{-1}$ and 10 $\mu S~cm^{-1}$). The observed trend is anticipated,

as pDEP is known to be more effective in a low-conductivity medium, hence the relatively frequent occurrence of trapping beads in groups. With a low-conductivity medium, the chances of trapping beads individually and in pairs were equally high as well. Although the probability of a single-particle positioning is more likely to occur in a medium of 1000 μS cm^{-1}, this conductivity becomes ineffective after switching the electrodes to a lower conductivity electrolyte (15 mS cm^{-1}), which is more relevant to biological applications. Thus, in the subsequent experiments, the conductivities were fixed at 100 μS cm^{-1} and 15 mS cm^{-1}, respectively, for the bead/cell medium and the electrodes. The former is on the low end to which many cell types can tolerate for a brief period of exposure while the latter offers a reasonable approximation to the intracellular conductivity often utilized in the cell experiments. Lowering the conductivity of the electrolyte for the electrodes to 15 mS cm^{-1} slightly increased the trapping statistics of beads in pairs or groups at a microcapillary [Fig. 3(c)].

Minimum trapping voltage. The requirement of a minimum voltage for trapping a bead flowing at a constant speed was empirically determined. Fig. 4 depicts a representative trapping event of a single 10 μm bead moving at a speed of 0.5 mm s^{-1} through superimposed images as the bead gets trapped at a microcapillary under pDEP (22.4 V-rms, 500 kHz, Supplementary, Video I†). Fig. 4 also presents the measurements in a plot indicating a linear correlation between the minimum trapping voltage that needs to be applied to the electrodes and the initial speed of the beads. The beads moving at a rate below 1 mm s^{-1}, which is typical of many microfluidic applications, can be trapped
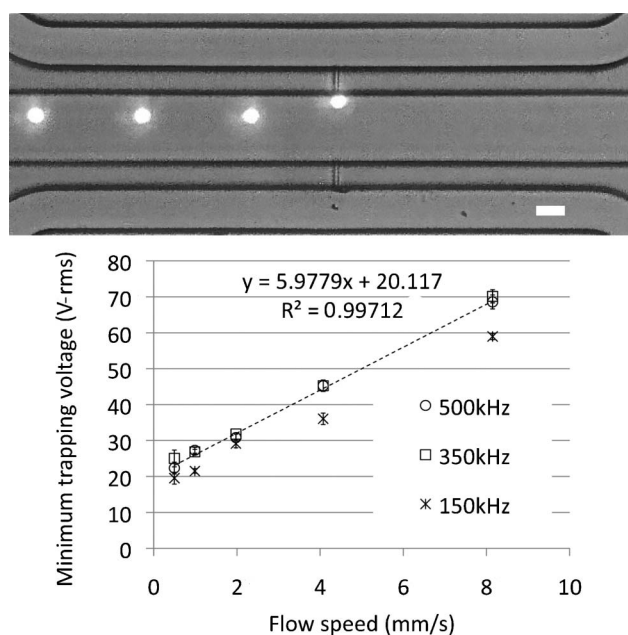

$$y = 5.9779x + 20.117$$
$$R^2 = 0.99712$$

Fig. 4 Superimposed images of a single fluorescent bead moving at a speed of 0.5 mm s^{-1} being positioned at a microcapillary under pDEP forces (excitation: 22.4 V-rms at 500 kHz). Scale bar: 20 μm. Shown in the plot is the minimum voltage (at different drive frequencies) required for trapping a single bead cruising at different speeds. Each data symbol and the respective error bar indicate the mean and ±1 standard deviation of five repeat measurements.

by a minimum voltage of 20–30 V-rms while those at a faster pace require accordingly higher voltages increasing at a rate of ~6 V-rms for every increment of 1 mm s^{-1}. Such rate of increase is necessary for higher frequencies (350 kHz, 500 kHz) but slightly exceeds the required values for lower frequencies (150 kHz). This is because the microcapillaries are more effective traps when the field lines are mostly channeled and squeezed through them, which occurs at lower frequencies, rather than the field lines capacitively-coupled through the dielectric partitions at higher frequencies.

Cell experiments

To demonstrate capability of the microcapillary-assisted DEP, we also used it to position cells. Fig. 5a depicts through superimposed images a representative trapping of a single CHO cell while moving at a speed of 40 μm s^{-1} (35 V-rms, 500 kHz) and another cell being already captured at the opposing microcapillary. Compared to beads, cells typically demanded a higher trapping voltage at a comparable flow speed. We did not encounter cells getting trapped in groups except those forming pearl chains (Supplementary, Videos II and III†). Very often, though, a cell after being successfully trapped could be dislodged and displaced from the trap by an incoming cell having sufficient momentum despite the fact that the activation voltage was constantly applied. We also noticed that the activation voltage had to be kept on to hold a cell against the flow. Throughout the experiments, we did not observe any sign of cells being lysed or disintegrated, generally the concern over holding cells at the field maximum (under pDEP).

To further investigate the impact of the method on the viability of cells, we conducted experiments on calcein-loaded cells. Fig. 5b shows a plot of fluorescence intensities measured over time from individual cells being trapped under distinct magnitudes of voltage excitation constantly applied at 500 kHz as well as from those in microchannels that did not experience any electric field (controls). The controls and the cells trapped by 35 V-rms exhibited a similar rate of decay in their fluorescence over the same time scale (axis above the graph) whereas those trapped by 141 V-rms began to loose their fluorescence at a much faster rate (the axis below the graph), suggesting electroporative release of calcein. Nevertheless, all the cells remained intact throughout the observations. Based on the results, we conclude that significant and rapid electroporation may take place at high operating voltages while relatively low yet practical voltages (e.g., 35 V-rms) could be safe to use with μC-DEP. This may be unexpected given that small voltage pulses (<1 V) were shown to electroporate cells trapped at similar microcapillaries as a result of focusing the electric field intensity across the portion of cell membrane.[10] However, such pulses last for a sufficient period of time (milliseconds).[10] The duration with which a voltage pulse exceeds a threshold level is a critical parameter for an effective cell electroporation.[28,29] These pulses typically last hundreds of microseconds to tens of milliseconds. With a sine wave applied here at 500 kHz, each uninterrupted excursion into the-above threshold potential is extremely short lived (<1 μsec) during either voltage polarity. Further-more, theoretical predictions require that a field intensity of 10 kV cm^{-1} be applied to electroporate cells using 1 μsec short rectangular pulses in a medium of a low conductivity buffer such
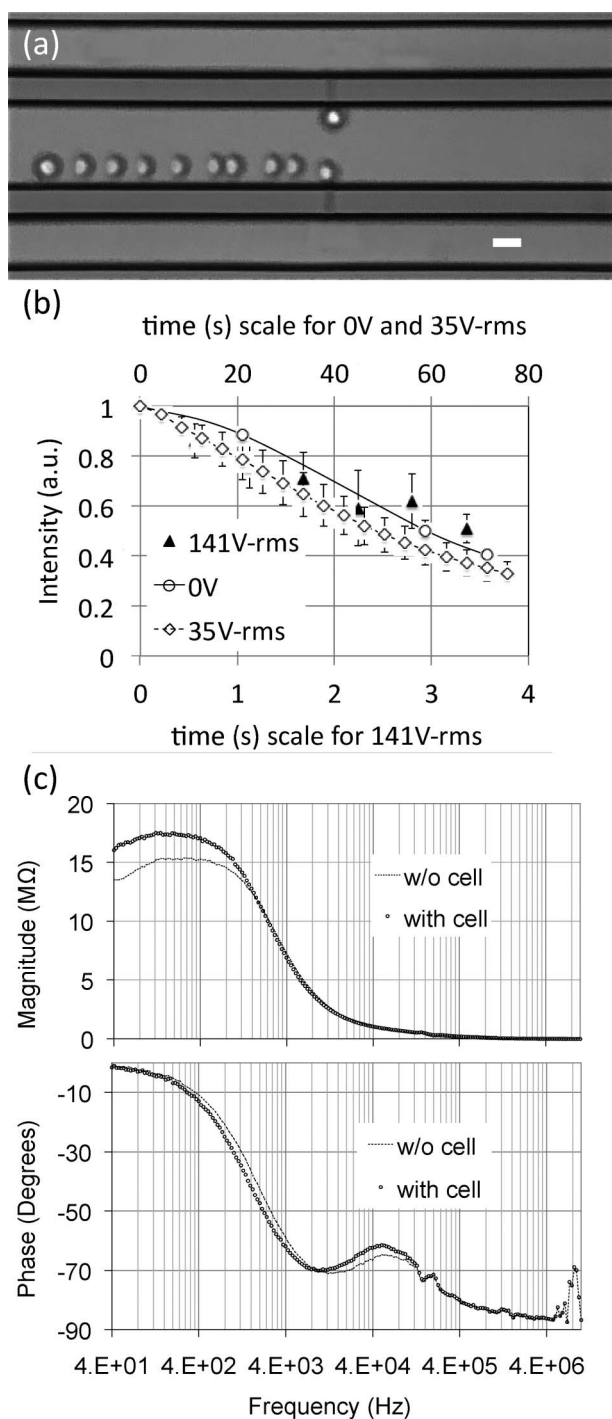
as the one used here.[30] It is reasonable to expect that the required field intensity could be even higher for a sine wave.[28,31]

A representative impedance spectrum of a cell is shown in magnitude and phase plots in Fig. 5c. The cell was positioned at a microcapillary by applying 35 V-rms at 500 kHz, as in Fig. 5a except without a second cell occupying the microcapillary across. Impedance measurements were taken across the two microcapillaries and subsequently repeated after removing the cell. The activation voltage was turned off during the measurements. The presence of the cell becomes apparent in the plots, particularly the magnitude at low frequencies (<1.4 kHz), with a relative change as high as ~20% in both the magnitude and the phase. Interestingly, in the mid-range frequencies (<50 kHz), the measurements with the cell are slightly lower than those without the cell possibly due to the fact that a lesser impedance is imposed by the cell membrane (electrically transparent) and the cell cytoplasm (two orders of magnitude more conductive than the medium). Throughout the high frequency region, the least resistance passage through the cell was overtaken by alternative paths penetrating through the dielectric partitions.

Our results confer with the previous single cell measurements although the measurements reported vary greatly depending on the cell type and the trap design.[7–9,32–38] A single breast cancer cell (MCF-7) placed near surface electrodes caused an increase from 10.9 MΩ to 12 MΩ at 1 kHz.[32] A liver carcinoma cell (HepG2) led to a ~10% rise in the magnitude at 1 kHz while up to 35% at 10–100 kHz.[33] A red blood cell showed nearly an order of magnitude increase from a baseline at <100 kΩ.[34] A single kidney cell (MDCK) changed the magnitude by 20–30%.[35] A cervical cancer cell (HeLa) in a hydrodynamic trap led to an increase of 20–30% at 300 kHz.[9] As can be seen, these changes are generally weak and occasionally unobservable even in the presence of multiple cells.[36] To boost the changes through a more intimate contact with a cell, researchers used surface-modified microelectrodes and observed an increase ~40% for individual fibroblast cells (NIH3T3) at 1 kHz.[37] Alternatively, researchers applied suction and yet encountered mixed outcomes: an increase of ~50% for a cell (L292) secured on a planar micro-hole[7] whereas statistically indistinguishable results for distinct cancer cells held against lateral traps.[38] We also applied gentle suction in the experiments upon positioning cells under pDEP and yet did not witness a considerable change in the impedance possibly due to the unique position of the microcapillaries which made them inaccessible to cells even with the suction applied. The microcapillaries moulded here posed a rectangular profile and hence it is reasonable to expect a substantial increase in the impedance magnitude for cells trapped when the technique applied through cylindrical glass microcapillaries integrated on silicon owing to their smooth and round opening.[4]

Other hydrodynamic traps demonstrated thus far for single bead/cell positioning are related to the microcapillary structures presented here except that they substitute the microcapillaries with larger constrictions.[39] Recently, researchers transformed these passive elements into active DEP traps by integrating them with surface microelectrodes. However, these designs induce particularly nDEP such that they can only eject or exclude beads/cells from the traps.[40]

Fig. 5 (a) Superimposed images of a single CHO cell moving at a speed of 40 μm s^{-1} being captured at a microcapillary (the lower partition) under pDEP forces (excitation: 35 V-rms at 500 kHz) while another cell is shown already trapped at the upper microcapillary. Scale bar: 20 μm. (b) Fluorescence intensities measured over time from individual cells trapped by either 35 V-rms or 141 V-rms, both applied at 500 kHz, and from those (control group) in the absence of excitation voltage (0 V). Note the use of dual axes (above and below the graph) to represent the curves of different time scales within the same graph. Each data symbol and the respective error bar indicate the mean and ±1 standard deviation of the measurements from four (control) or ten (pDEP trapped) individual cells. (c) Plots showing the magnitude and phase of an impedance spectrum obtained from a representative cell trapped at the microcapillary under pDEP (excitation: 35 V-rms at 500 kHz).

Conclusion

µC-DEP is demonstrated as a highly effective simple approach for precise and rapid positioning of particles and cells. The method bridges the two known sister techniques, iDEP and cDEP, leveraging their simplistic microfabrication, which is free from integrating solid electrodes. Unlike iDEP, which has to work with the conductivity of the sample medium, µC-DEP makes use of a dedicated medium for the electrodes and segregates the two through dielectric partitions with built-in microcapillaries. Unlike cDEP, this segregation does not lead to complete isolation of the electrodes and allows for a more effective electrical coupling through the microcapillaries. The microcapillaries also offer fluidic decoupling through their high hydrodynamic resistance. Above all, the method presented addresses the limitations in trapping cells *via* hydrodynamic suction. In conclusion, µC-DEP can be a simple and powerful tool for particle positioning in single-cell/bead dynamic assays.

Acknowledgements

References

1 J. Seo, C. Ionescu-Zanetti, J. Diamond, R. Lal and L. P. Lee, *Appl. Phys. Lett.*, 2004, **84**(11), 1973.
2 C. Ionescu-Zanetti, R. M. Shaw, J. Seo, Y. N. Jan, L. Y. Jan and L. P. Lee, *Proc. Natl. Acad. Sci. U. S. A.*, 2005, **102**(26), 9112.
3 W. L. Ong, J. S. Kee, A. Ajay, R. Nagarajan, K. C. Tang and L. Yobas, *Appl. Phys. Lett.*, 2006, **89**(9), 093902.
4 W. L. Ong, K. C. Tang, A. Agarwal, R. Nagarajan, L. W. Luo and L. Yobas, *Lab Chip*, 2007, **7**, 1357.
5 K. C. Tang, J. Reboud, Y. L. Kwok, S. L. Peng and L. Yobas, *Lab Chip*, 2010, **10**, 1044.
6 A. Han and A. B. Frazier, *Lab Chip*, 2006, **6**, 1412.
7 S. Cho and H. Thielecke, *Biosensors and Bioelectronics*, 2007, **22**, 1764.
8 J. Chen, Y. Zheng, Q. Tan, Y. L. Zhang, J. Li, W. R. Geddie, M. A. S. Jewett and Y. Sun, *Biomicrofluidics*, 2011, **5**, 014113.
9 D. Malleo, J. T. Nevill, L. P. Lee and H. Morgan, *Microfluidics and Nanofluidics*, 2010, **9**, 191.
10 M. Khine, A. D. Lau, C. Ionescu-Zanetti, J. Seo and L. P. Lee, *Lab Chip*, 2005, **5**, 38.
11 J. Castillo-Leon, W. E Svendsen and M. Dimaki, *"Micro and nano techniques for the handling of biological samples,"*, 2012, CRC Press, Boca Raton, FL.
12 R. Pethig, *Biomicrofluidics*, 2010, **4**, 022811.
13 K. Khoshmanesh, S. Nahavandi, S. Baratchi, A. Mitchell and K. K. Zadeh, *Biosens. Bioelectron.*, 2011, **26**, 1800.
14 B. Cetin and D. Li, *Electrophoresis*, 2011, **32**, 2410.
15 Z. R. Gagnon, *Electrophoresis*, 2011, **32**, 2466.
16 A. Rosenthal and J. Voldman, *Biophys. J.*, 2005, **88**, 2193.
17 R. S. Thomas, H. Morgan and N. G. Green, *Lab Chip*, 2009, **9**, 1534.
18 D. S. Gray, J. L. Tan, J. Voldman and C. S. Chen, *Biosens. Bioelectron.*, 2004, **19**, 1765.
19 G. Fuhr, W. M. Arnold, R. Hagedorn, T. Muller, W. Benecke, B. Wagner and U. Zimmermann, *Biochim. Biophys. Acta*, 1992, **1108**, 215.
20 T. Schnelle, R. Hagedorn, G. Fuhr, S. Fiedler and T. Muller, *Biochim. Biophys. Acta*, 1993, **1157**, 127.
21 C.-F. Chou, J. O. Tegenfeldt, O. Bakajin, S. S. Chan, E. C. Cox, N. Darnton, T. Duke and R. H. Austin, *Biophys. J.*, 2002, **83**, 2170.
22 H. Shafiee, J. L. Caldwell, M. B. Sano and R. V. Davalos, *Biomed. Microdevices*, 2009, **11**, 997.
23 H. Shafiee, M. B. Sano, E. A. Henslee, J. L. Caldwell and R. V. Davalos, *Lab Chip*, 2010, **10**, 438.
24 C.-P. Jen and T.-W. Chen, *Biomed. Microdevices*, 2009, **11**, 597.
25 S. Bhattacharya, T.-C. Chao and A. Ros, *Electrophoresis*, 2011, **32**, 2550.
26 H. A. Pohl, *Dielectrophoresis*, Cambridge University Press, London, 1978.
27 J. L. Griffin and C. D. Ferris, *Nature, 226*, 152, 1970.
28 T. Kotnik, G. Pucihar, M. Rebersek, D. Miklavcic and L. M. Mir, *Biochimica Et Biophysica Acta-Biomembranes*, 2003, **1614**(2), 193.
29 M. P. Rols and J. Teissie, *Biophysical J.*, 1998, **75**(3), 1415.
30 T. Kotnik, F. Bobanovic and D. Miklavcic, *Bioelectrochemistry and Bioenergetics*, 1997, **43**(2), 285.
31 E. Neumann, A. E. Sowers and C. A. Jordan, *"Electroporation and electrofusion in cell biology,"* 1989, Plenum Press, New York.
32 H. Park, D. Kim and K. Yun, *Sens. Actuators B Chem.*, 2010, **150**, 167.
33 V. Senez, E. Lennon, S. Ostrovidov, T. Yamamoto, H. Fujita, Y. Sakai and T. Fujii, *IEEE Sensors*, 2008, **8**(5), 548.
34 Y. H. Cho, T. Yamamoto, Y. Sakai, T. Fujii and B. Kim, *J Microelectromech. Sys.*, 2006, **15**(2), 287.
35 S. Z. Hua and T. Pennell, *Lab Chip*, 2009, **9**, 251.
36 C. Tlili, K. Reybier, A. Géloën, L. Ponsonnet, C. Martelet, H. B. Ouada, M. Lagarde and N. Jaffrezic-Renault, *Anal. Chem.*, 2003, **75**, 3340.
37 M. Thein, F. Asphahani, A. Cheng, R. Buckmaster, M. Q. Zhang and J. Xu, *Biosens. Bioelectron.*, 2010, **25**, 1963.
38 Y. Cho, H. S. Kim, A. B. Frazier, Z. G. Chen, D. M. Shin and A. Han, *J. Microelectromech Syst.*, 2009, **18**, 808.
39 W.-H. Tan and S. Takeuchi, *Proc. Natl. Acad. Sci. U. S. A.*, 2007, **104**(4), 41146.
40 B. M. Taff, S. P. Desai and J. Voldman, *Appl. Phys. Lett.*, 2009, **94**, 084102.